^{20}Ne-induced reactions with Cu and ^{197}Au at 8.6 and 12.6 MeV/nucleon

G. J. Mathews
Lawrence Livermore National Laboratory, University of California, Livermore, California 94550

J. B. Moulton,* G. J. Wozniak, B. Cauvin,† R. P. Schmitt,‡ J. S. Sventek,§ and L. G. Moretto
Nuclear Science Division, Lawrence Berkeley Laboratory, University of California, Berkeley, California 94720

(Received 3 September 1981)

Products from the reactions of 170- and 252-MeV ^{20}Ne with ^{nat}Cu and ^{197}Au have been studied. The charge and angular distributions of the Z-identified fragments are discussed in terms of diffusion along the mass-asymmetry coordinate. This diffusion model has been generalized to include the effects of shape evolution, which is important for these deeply penetrating systems, and also the effect of N/Z equilibration, which is important for highly asymmetric systems such as ^{20}Ne + ^{197}Au.

[NUCLEAR REACTIONS ^{nat}Cu, ^{197}Au(^{20}Ne,Z), E=170 and 252 MeV. Measured $\sigma(E,Z,\theta)$, for $6 \leq Z \leq 30$. Theoretical interpretation based on a diffusion model.]

I. INTRODUCTION

Reactions induced by ^{20}Ne are of particular interest in the study of a number of aspects of heavy-ion collisions. The Coulomb and the centrifugal barriers are typically small compared to those involving heavier projectiles at the same energy over the barrier, so that in Ne-induced reactions one expects deeper internuclear penetration. Therefore, these reactions are of interest in the study of the deep-inelastic[1-7] and complete-fusion[8,9] processes. Another interesting feature of ^{20}Ne induced collisions, which was pointed out in studies of the ^{20}Ne + ^{107,109}Ag reaction,[3] is that the entrance channel configuration is usually very near the Businaro-Gallone maximum of the potential energy as a function of mass asymmetry. Thus, the mass transport between the projectile and target may be sensitive to this aspect of the ridge-line potential energy.[3] In this paper results are reported from measurements of fragment energy, charge, and angular distributions for the reactions 170- and 252-MeV ^{20}Ne + ^{nat}Cu and 175- and 252-MeV ^{20}Ne + ^{197}Au.

Some parameters which are useful in characterizing these reaction systems are summarized in Table I. A relevant parameter is the ratio of center-of-mass energy to the Coulomb barrier (E/B) at the interaction radius. As pointed out previously,[10,11] small values of E/B ($\lesssim 1.5$) are generally associated with the side-peaked angular distributions and the narrow mass distributions observed in fairly heavy projectile-target systems, whereas larger values of E/B are associated with

TABLE I. Some parameters which characterize the reaction systems. E/B is the ratio of center-of-mass energy to Coulomb barrier at the interaction radius ($R_1 + R_2 + 3.2$ fm), l_{max} and θ_G are the grazing angular momentum and angle, respectively.

Reaction	E_{lab} (MeV)	$E_{c.m.}$ (MeV)	E/B	$l_{max}(\hbar)$	$\theta_{G(c.m.)}$	$(N/Z)_{proj}$	$(N/Z)_{tgt}$	$(N/Z)_{system}$
^{20}Ne + ^{63,65}Cu	170	130	3.2	83	21°	1.0	1.21	1.15
	252	192	4.8	108	13°	1.0	1.21	1.15
^{20}Ne + ^{197}Au	175	159	1.8	97	46°	1.0	1.49	1.44
	252	229	2.6	138	28°	1.0	1.49	1.44

the forward-peaked angular distributions and the broad mass distributions often observed in lighter systems. For the ^{20}Ne + ^{nat}Cu system at 170 and 252 MeV bombarding energy, E/B is 3.2 and 4.8, respectively (see Table I). Thus this system should exhibit forward-peaked angular distributions at both bombarding energies. The lower E/B ratios for ^{20}Ne + ^{197}Au lead to the possible expectation of side-peaked angular distributions for the 175 MeV bombarding energy.

These ^{20}Ne + ^{nat}Cu data are also interesting because complementary data exist for the light-fragment and evaporation-residue yields,[2] charged particle emission,[6,7] and γ-ray multiplicity[2,5] for this system. These data plus the singles data presented herein, should allow for a fairly complete picture of the ^{20}Ne + ^{nat}Cu reaction. An interesting feature of the ^{20}Ne + ^{197}Au system is the substantial difference between the N/Z ratio of the projectile and the target (see Table I). This system may show effects due to the fast N/Z equilibration process. Of course, in order to study this process in detail, one needs simultaneous Z and A measurements, nevertheless, some possible evidence of the fast N/Z equilibrium may be seen in these Z-identified data.

Details of the experimental technique are discussed in Sec. II. The kinetic-energy spectra, charge distributions, and angular distributions are discussed in Secs. III, IV, and V, respectively. In Sec. VI, the evolution of the system along the mass asymmetry coordinate is described in terms of a diffusion model which is an extension of the model of Moretto and Sventek.[12–14] In particular, this new model eliminates some of the free parameters associated with the collision dynamics, and includes a treatment of both the shape evolution and N/Z equilibrium of the dinuclear system. In Sec. VII, the data are interpreted in terms of this diffusion model and compared with model calculations.

II. THE EXPERIMENT

The ^{20}Ne beams were obtained from both the LBL SuperHILAC and 88″ cyclotron. The targets consisted of self-supporting natural ($\sim$400 μg/cm^2) Cu and ($\sim$900 μg/cm^2) Au foils. Typical beam currents were $\sim$30 na electrical, and typical beam spot sizes were less than 3 mm diameter. Reaction products were identified with two ΔE (gas)-E (silicon) telescopes[15] placed about 10 cm from the target on movable arms. The telescope acceptance angles, which ranged from 1 to 2.5°, were defined by circular collimators 1 to 3 mm in diameter. The absolute solid angles were determined with an ^{241}Am α source of known activity.

An energy calibration of the E-amplifier systems was obtained from a precision mercury pulser that was calibrated at low energies with an ^{241}Am α source and at high energies with elastically scattered ^{20}Ne ions. The ΔE amplifier systems were calibrated utilizing the mercury pulser and measuring the shift of the elastic scattering peak in the E detector (and the corresponding amplitude in the ΔE detector) for runs with and without gas in the telescope. The laboratory energies of the fragments were corrected for losses in the target and window of the gas counter using polynomial fits to Northcliffe and Schilling range-energy data.[16] Although the relative energies are known to better than one percent, the laboratory energy of the fragments could be in error by as much as two percent.

The detector signals were routed through standard linear and logic circuitry, and were serialized and digitized with a multiplexer and a 4096-channel analog-to-digital converter. The digital information together with marker bits identifying the telescopes, were written onto magnetic tape in an event-by-event format.

To identify the atomic number (Z) of the reaction products, the event-by-event data were sorted into two-dimensional ΔE vs E maps (960×100 channels). An example of such a map for the 170-MeV ^{20}Ne + ^{nat}Cu reaction is shown in Fig. 1. Ridges corresponding to individual atomic numbers are clearly identifiable up to $Z\simeq25$. A computerized algorithm[17] was used to automatically locate these ridges. The absolute Z calibration was provided by the prominent projectile ridge.

III. KINETIC ENERGY SPECTRA

Individual energy spectra for each Z value were obtained by defining the boundary line between two adjacent ridge lines in the ΔE-E map. The energy corrections were made and the spectra were then edited for various experimental artifacts, which are visible on the ΔE-E map (cf. Fig. 1). One such feature is the background in the energy spectrum for the projectile caused by collimator scattering. Another such feature is the tendency of the higher mass products ($Z>26$) to merge together at low energies producing a low energy spike in the energy spectra.

Representative center of mass (c.m.) energy spec-

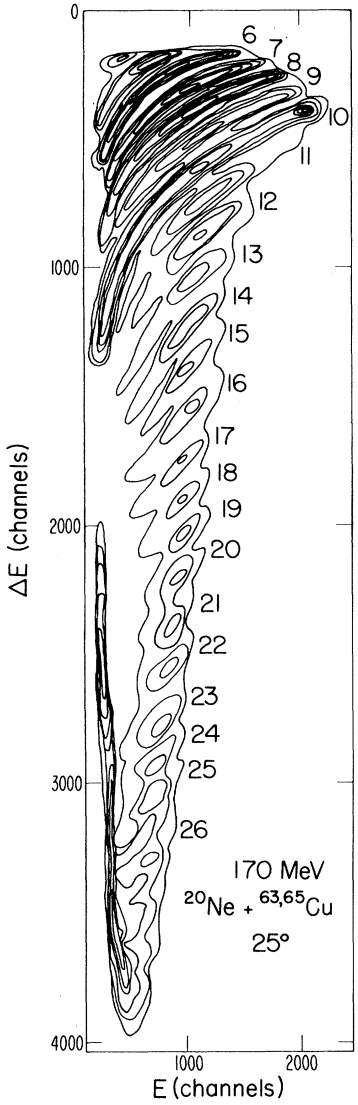

FIG. 1. A ΔE vs E map showing contour lines of constant cross section. This map was obtained from the 170-MeV ^{20}Ne + ^{nat}Cu reaction at 25° in the laboratory. The identification of individual atomic numbers up to $Z \simeq 25$ is clearly visible.

tra from the 170-MeV Ne + ^{nat}Cu reaction at three lab angles are shown in Fig. 2. These spectra have been converted to c.m. spectra by assuming binary kinematics and fragment masses which minimize the total liquid-drop potential energy of the two fragments in contact. These spectra exhibit the well known features of deep inelastic reactions: a Gaussian-shaped relaxed component at all angles and for all atomic numbers, and a higher energy quasielastic component at forward angles near the grazing angle (see Table I) for atomic numbers

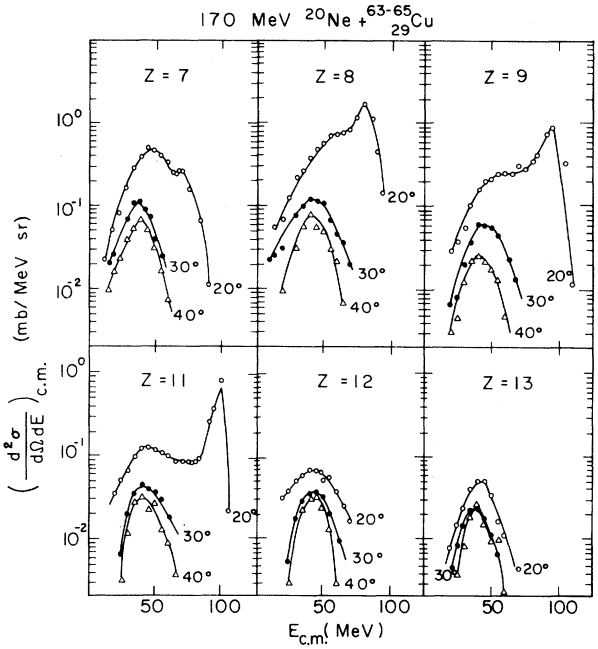

FIG. 2. Center-of-mass kinetic energy spectra at three angles for fragments produced in the 170-MeV ^{20}Ne + ^{nat}Cu reaction.

near the projectile. In the center-of-mass, the centroid of the relaxed component roughly corresponds to the Coulomb energy for touching fragments. The relaxed component of these spectra was separated from the quasielastic component by fitting two Gaussians to the spectrum.

Centroids and widths of the kinetic-energy spectra, averaged over the experimental angular range, from the ^{20}Ne + ^{197}Au reaction (corrected for neutron emission[18]) are shown in Fig. 3. Liquid-drop model calculations[18] are shown for the mean energies which assume that the scission configuration can be approximated as two rotating, vibrating, colinear spheroids in contact with each other, and in statistical equilibrium. The ^{20}Ne + ^{nat}Cu data (not shown) exhibit similar behavior. The overall reproduction of the data, from the ^{20}Ne + ^{197}Au reaction, is consistent with the assumption of a binary reaction mechanism for the formation of these fragments. Although some of the heavier fragments could conceivably be produced[18] by sequential fission of the Au-like fragment following a deep-inelastic collision, a recent study[19] of the sequential fission of Au-like fragments produced in the 252 MeV ^{20}Ne + ^{197}Au reaction indicates that the contribution to the charge distribution from this process is probably small.

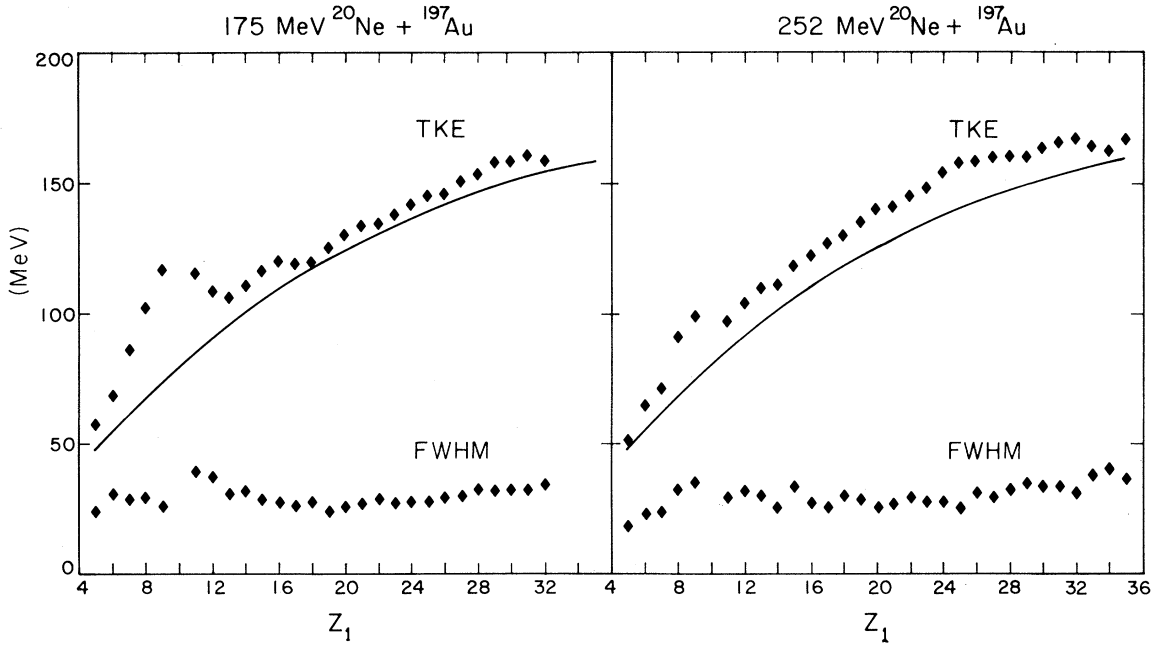

FIG. 3. Experimental angle averaged, center-of-mass kinetic energies (upper points) and full widths at half maximum (lower points) as a function of the fragment atomic number for products from the ^{20}Ne + ^{197}Au reaction at 175 and 252 MeV. Calculated values are given by smooth curves (see text).

IV. CHARGE DISTRIBUTIONS

The energy spectra were integrated to give cross sections for the deep-inelastic (DI) and quasielastic (QE) components. The charge distributions for different lab angles are shown in Figs. 4 and 5. The total angle-integrated (DI plus QE) charge distributions are shown in Figs. 6 and 7 for the lower-bombarding energy where enough data points were obtained to make a reasonable extrapolation of $(d\sigma/d\theta)_{\text{c.m.}}$ to 0° and 180°. The error bars shown on these latter two figures essentially reflect the uncertainty in the extrapolations to 0°, which are most uncertain for products near the projectile. The 170-MeV ^{20}Ne + $^{\text{nat}}$Cu data reported here are quite similar to the 166-MeV ^{20}Ne + ^{63}Cu results reported in Ref. 2.

Several features in Figs. 4—7 merit discussion. One is the distinct difference between the trends in the ^{20}Ne + $^{\text{nat}}$Cu and ^{20}Ne + ^{197}Au data at symmetry. While the cross section for products from the Cu bombardment exhibit a distinct minimum near or somewhat below symmetry ($Z \simeq 19$), the yield of products from the Au bombardment first decreases for Z values above the projectile but then increases toward symmetry ($Z \simeq 44$). For the Ne + Au reaction the symmetric products are likely to be the re-

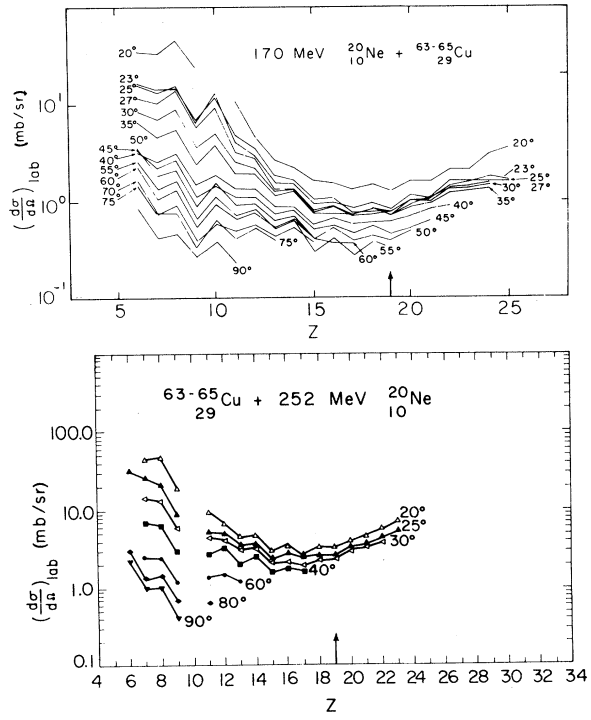

FIG. 4. Charge distributions at various laboratory angles for the relaxed component alone in the 170- and 252-MeV ^{20}Ne + ^{63,65}Cu reactions. For this system symmetry is indicated by the arrows.

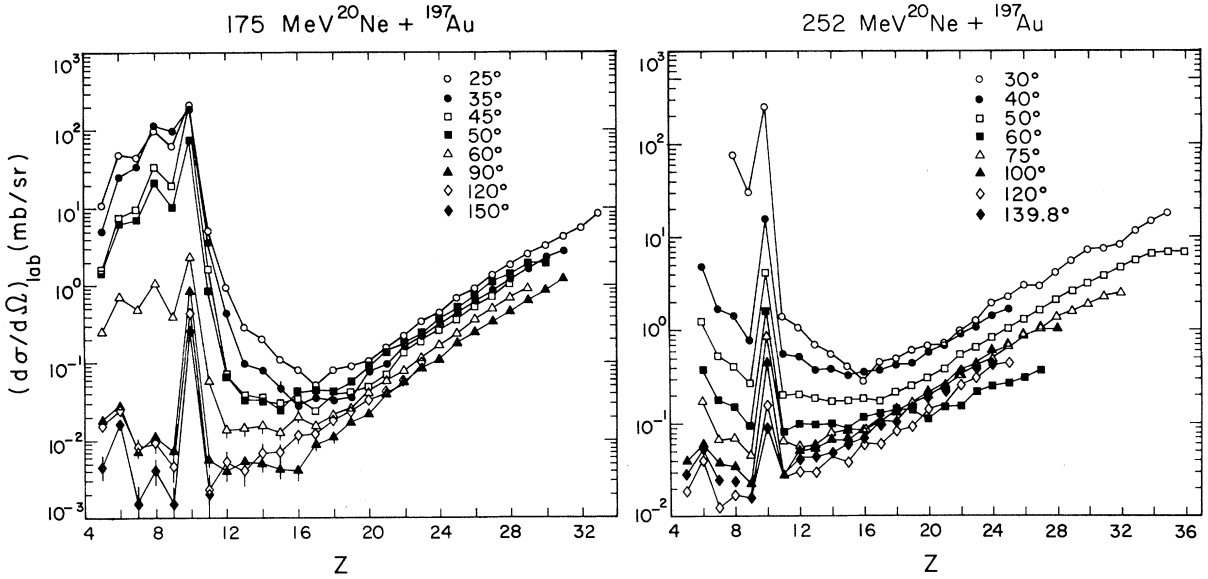

FIG. 5. Charge distributions at various laboratory angles integrated over both the relaxed and quasielastic components in the 175- and 252-MeV ^{20}Ne + ^{197}Au reactions.

sult of the fusion-fission process (not necessarily preceded by compound nucleus formation). For the ^{20}Ne + ^{nat}Cu reaction, the entrance-channel mass asymmetry is below the Businaro-Gallone point[3,11] (at least for the lowest l waves), and therefore, an asymmetric mass distribution with a minimum at symmetry is expected even for fusion-fission events.

An increase in the yield of the DI component and broadening of the charge distribution is observed at the larger bombarding energy for both systems. These trends can be attributed to the larger number of l waves and to the increased average temperature associated with the higher bom-

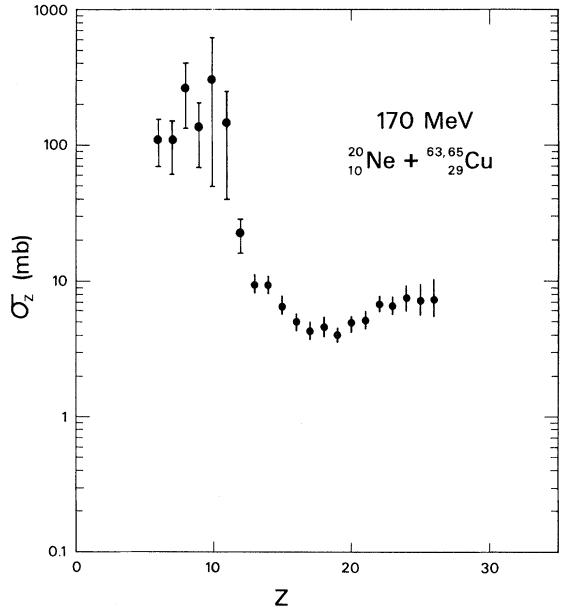

FIG. 6. The angle-integrated charge distributions of the DI and QE products from the 170-MeV ^{20}Ne + ^{63,65}Cu reaction. See text.

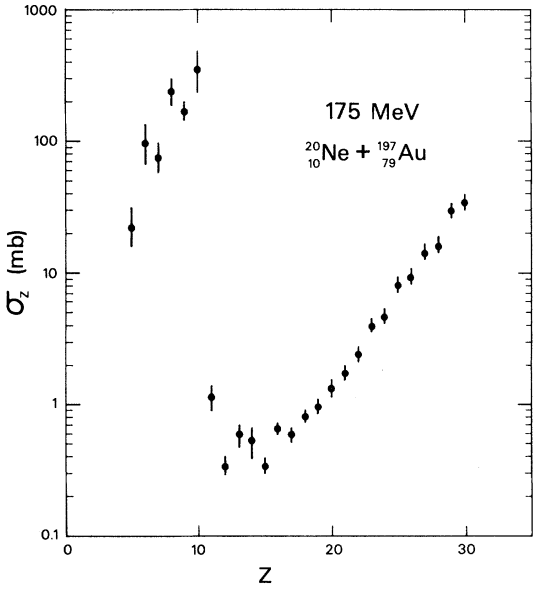

FIG. 7. The angle-integrated charge distribution of the DI and QE products from the 175-MeV ^{20}Ne + ^{197}Au reaction. See text.

barding energies. Another feature evident in the charge distributions, particularly for the ^{20}Ne + ^{nat}Cu system, is the odd-even effect. As suggested by the calculations of J. Gomez del Campo,[20] this effect may result from the preferential population of even atomic numbers during particle evaporation following the collision process.

Another feature of the charge distributions is the striking asymmetry about the projectile Z value. The cross section is high below $Z=10$, but falls off rapidly above $Z=10$. This feature is most pronounced at forward angles where the quasielastic component dominates the cross section. However, an asymmetry is observed even at backward angles where there is no contribution from quasielastic reactions. It is difficult to interpret this trend in terms of the ridge-line potential, especially for the ^{20}Ne + ^{197}Au reaction. Since the ridge-line potential energy for the ^{20}Ne + ^{197}Au system would produce a drift toward symmetry, the enhanced yield for $Z \lesssim 10$ is not likely to be due to equilibration of the mass asymmetry degree of freedom. An explanation in terms of projectile fragmentation also seems unlikely, since this process in not expected to be important below 20 MeV/A bombarding energy.[21] One possible explanation may be the equilibration of the N/Z ratio of the fragments. Since there are fewer protons than neutrons available, especially for the ^{20}Ne + ^{197}Au system, the N/Z ratio can be more easily equilibrated by the transfer of protons from the projectile to the target nucleus. Numerous data exist [22,23] which demonstrate the short relaxation time for N/Z equilibration.

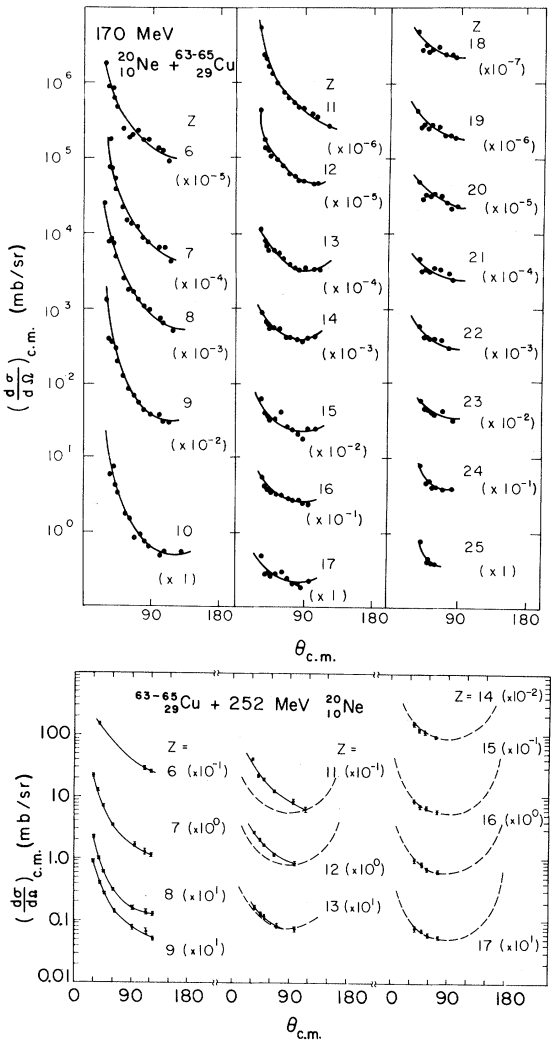

FIG. 8. Center-of-mass angular distributions of products for the 170- and 252-MeV ^{20}Ne + ^{63,65}Cu reactions. The dashed lines indicate a $1/\sin\theta$ distribution. For each Z value a scale normalization factor is given (i.e., for $Z=8$, $\times 10^{-3}$) which must be multiplied times the ordinate scale to read off the angular distribution in mb/sr.

V. ANGULAR DISTRIBUTIONS

The center-of-mass kinetic-energy spectra were integrated to give the angular distributions shown in Figs. 8 and 9. For the most part, these angular distributions are typical of deep inelastic scattering of light projectiles based on E/B systematics.[10,11] The angular distributions of products close to the projectile from the ^{20}Ne + ^{nat}Cu system are forward peaked. For smaller atomic numbers this forward peaking is quite strong, while for larger Z values, the angular distributions have a $1/\sin\theta$ appearance. The angular distributions from the ^{20}Ne + ^{197}Au system exhibit a similar dependence on Z value. For the 175-MeV reaction, however, there is also some evidence for a side peak for products near the projectile Z value. This side peaking in the angular distributions of the DI products can be understood in terms of the lifetime, moment-of-inertia, and rotation angle of the dinuclear system. In previous work[10,11] it was suggested that the onset of side peaking should be correlated with a ratio E/B of $\lesssim 1.5$. For the 175-MeV ^{20}Ne + ^{197}Au reaction, $E/B=1.8$ (see Table I). This value is only slightly larger than the transition value of 1.5 and confirms the approximate validity of this scaling parameter, but suggests that the side peaking persists to higher energies for more asymmetric systems.

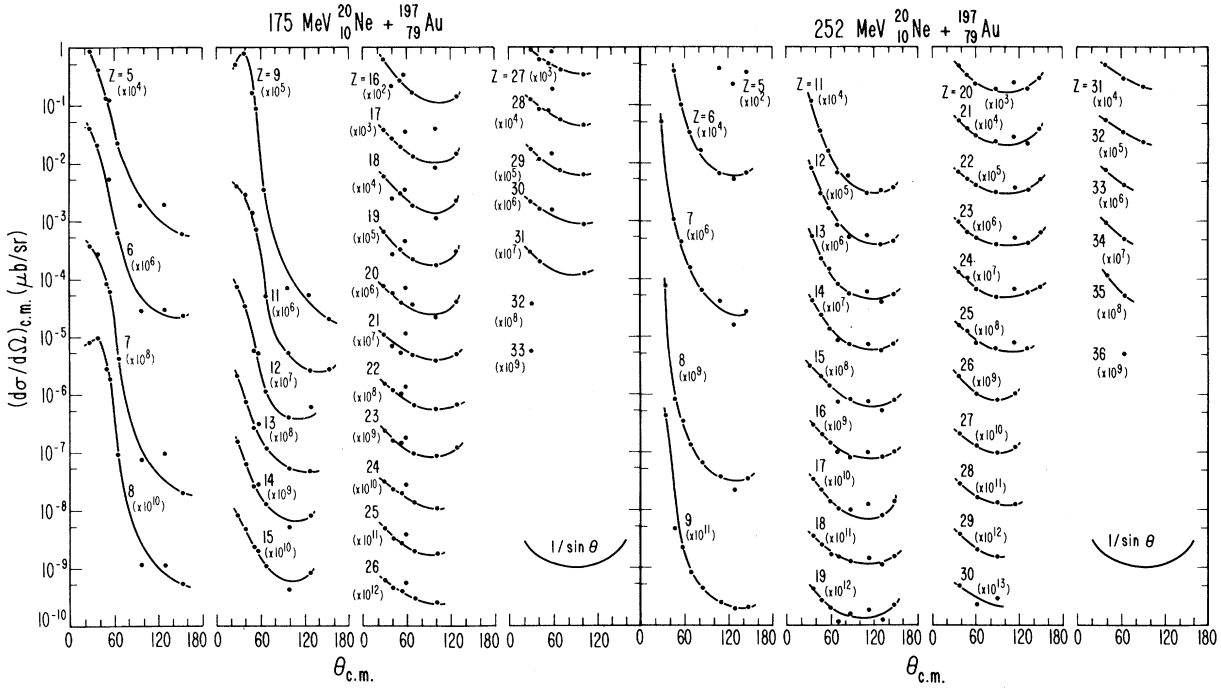

FIG. 9. Center-of-mass angular distributions of products for the 175- and 252-MeV ^{20}Ne + ^{197}Au reactions. For each Z value a scale normalization factor is given (i.e., for $Z=8$, $\times 10^{10}$) which must be multiplied times the ordinate scale to read off the angular distribution in μb/sr.

The overall pattern of the angular distributions as a function of Z value indicates that the lifetime of the dinuclear complex increases for exit channel asymmetries progressively removed from the entrance channel.[24] The fact that the distributions of products with Z values below that of the projectile are side or forward peaked implies that the average lifetime for the formation of these products is smaller than the average rotation period of the dinuclear system. The $1/\sin\theta$ distributions for the products farther removed from the projectile Z value indicate that these products are associated with substantially longer times ($\geq$ one rotation period), and with a lifetime distribution which is sufficiently broad to insure that no correlation exists with the initial angle. This will be discussed further in Sec. VII.

VI. THE MODEL

As discussed in the Introduction, several features of ^{20}Ne induced reactions (e.g., deeply penetrating and highly asymmetric) render the interpretation of the data in terms of simple phenomenological diffusion models[13,14,25] rather difficult. In this section, a generalized diffusion model is briefly described which can be applied to ^{20}Ne induced reactions.

A. Evolution along the mass asymmetry coordinate

The time evolution of the population Φ_A of a given asymmetry, A, for the system is treated using the master equation as discussed previously.[13,14] In our treatment we have assumed that the microscopic transition probability between asymmetries A and A' are of the form

$$\lambda_{AA'}=\frac{n_0\sigma\rho_{A'}(E-V_{A'})}{\rho_A(E-V_A)+\rho_{A'}(E-V_{A'})}\ , \tag{1}$$

where n_0 is the appropriate one-way flux of nucleons and σ is the area of the window between the fragments. These quantities are taken from the one-body proximity formulation.[12,26] A justification for this form for the transition probability is given in Ref. 27.

B. (N/Z) equilibrium

The correct way to describe the total dispersion due to mass transfer is to simultaneously solve the

master equation for both the neutron and proton degrees of freedom. To decrease the length and cost of the model calculations, we treat the two sources of dispersion independently, i.e., we compute the total dispersion in the charge distribution Φ_Z as a convolution of the dispersion due to N/Z equilibrium Φ_{NZ} and the dispersion Φ_A due to motion along the charge asymmetry coordinate,

$$\Phi_Z = \int \Phi_{NZ}(Z'-Z_0)\Phi_A(Z-Z')dZ' , \quad (2)$$

where Z_0 labels the entrance channel asymmetry. In practice, this expression is implemented by solving for Φ_{NZ} first, and then using this dispersion as the initial condition for the diffusion along the charge asymmetry coordinate.

Since the potential energy as a function of charge division is harmonic for fixed mass asymmetry, one can utilize the analytical solution[11] to the Fokker-Planck equation assuming that the drift and dispersion can be approximated by average values for a given impact parameter

$$\Phi_{NZ}(t) = \frac{1}{\sigma_{NZ}\sqrt{2\pi}} \times \exp\{ -[Z - Z_0\exp(-t/\tau_{NZ})]^2/2\sigma_{NZ}^2 \} , \quad (3)$$

where Z_0 is the entrance-channel asymmetry and τ_{NZ} is the mean lifetime for N/Z equilibrium. This quantity we estimate in a simple model where

$$\tau_{NZ} = \frac{TA_c}{2CZ_c n_0 \sigma} . \quad (4)$$

Here T is the average nuclear temperature during the collision and C is the curvature constant of the harmonic potential as a function of Z for fixed mass. The quantities A_C and Z_C are the mass and charge of the composite system. The ratio T/C is the thermal variance of the equilibrium distribution, and is therefore roughly a measure of the number of random charge transfers necessary to achieve equilibrium. The quantity $(2Z_c n_0 \sigma/A_c)$ is just the total rate of charge transfer. For the actual variance, σ_{NZ}^2, both a quantal[28] and a thermal width were included

$$\sigma_{NZ}^2 = \frac{\hbar\omega}{C}\left[\frac{1}{2} + \frac{1}{\exp(\hbar\omega/T)-1}\right] \times \left[1-\exp(-2t/\tau_{NZ})\right] . \quad (5)$$

C. Charge distributions

The final cross sections for each Z and l wave are given by

$$\frac{d\sigma_Z}{dl} = \sigma_{\rm tot}\frac{2l}{l_{\rm max}^2}\int \Phi_z(t)\Pi(t)dt , \quad (6)$$

where $\Pi(t)$ is a Gaussian lifetime distribution[14] centered at the mean lifetime τ_l and with a variance assumed proportional to τ_l. The mean lifetimes are estimated from the dynamics (see Sec. VI D). The proportionality constant in the lifetime variance is left as an adjustable parameter. The total reaction cross section $\sigma_{\rm tot}$ is assumed to be the geometrical cross section for the target and projectile separated by their half-density radii.[29,30]

D. The dynamics

The model requires several quantities which depend on the details of the dynamics of the system at different impact parameters. Besides the mean lifetime, these quantities include the average window area between the fragments, the rotation angle of the system, and the scission radius. Rather than treat these quantities as free parameters, they are estimated by solving the classical equations of motion for the entrance-channel asymmetry. The shape evolution of the system along with dissipative forces are included in a schematic way. We make use of recent ideas of Swiatecki[31] and of Randrup[32] on neck formation and its effect on mass transport. The neck between the two ions is treated as a cylinder. Neglecting volume conservation and the Coulomb energy of the cylinder, the contribution of this neck to the potential energy is then just the difference between the surface energy of the cylinder and the surface energy of the neck area of the two ions, with proper proximity corrections.

In this model the Rayleigh dissipation function (due to only one-body dissipation) can be written as

$$F = \frac{1}{2}\frac{dE}{dt} = 2\pi n_0\sigma(\dot{r}^2 + \tfrac{1}{2}u_t^2) + 4\pi n_0 \ln\dot{n}^2 , \quad (7)$$

where n_0 is the one-way nucleon flux (taken here as 0.243×10^{22} nucleons fm^{-2}s^{-1}). The quantities l and n are the length and radius of the neck, respectively, and the quantity σ is the effective window between the fragments

$$\sigma=\pi n^2+2\pi\bar{R}b\Psi(l/b)\exp(-n^2/2\bar{R}b)\ , \qquad (8)$$

where $\Psi(l/b)$ is the dimensionless proximity current[26] and $\bar{R}$ is the reduced radius. The first term in Eq. (7) corresponds to one-body (window formula[33]) dissipation. The second term is just the dissipation associated with motion of the wall of the cylindrical neck (wall formula[33]).

Neck formation is assumed to occur when the overlap density of the two ions equals the half-density. This occurs at a separation of about 1.73 fm for a trapezoidal density distribution.[31] The window radius for this geometric limit of minimum neck formation as a function of separatrion s between the half-density radii of the two surfaces is just

$$n_g=\sqrt{2\bar{R}(1.73-s)}\ . \qquad (9)$$

Typically, the growth of the neck will be characterized by a rapid motion along this geometrical limit until near the classical turning point. When the ions begin to separate, the collapse of the neck is then hindered by one-body dissipation.[33] While integrating the equations of motion, we also compute the average values of the window area and the excitation energy needed for the charge diffusion calculation.

E. Rotation angles and final angular momenta as a function of asymmetry

In addition to the entrance-channel trajectory described above, one also needs trajectories for events where there is a net mass transfer, which may deviate significantly from the entrance-channel trajectory. To compute the potential energy and transition probabilities as a function of asymmetry, we assume that the average overlap is constant and that the neck radius scales[31] with the reduced radius. The average excitation energy is taken as $E_Z^*=\langle E^*\rangle+V_{Z_0}-V_Z$, where Z_0 is the entrance channel asymmetry and $\langle E^*\rangle$ is the average excitation energy for the entrance channel asymmetry. To compute rotation angles and final angular momenta as a function of asymmetry, the angular equations of motion[34] are solved for every asymmetry assuming that the average overlap is constant and that the moment of inertia varies linearly in time from the entrance-channel value to the final value.

VII. RESULTS

A. Lifetimes

Calculated mean lifetimes for the ^{20}Ne + ^{nat}Cu and ^{20}Ne + ^{197}Au reactions are shown in Figs. 10 and 11 as a function of incident l wave. Results are presented for calculations with and without neck formation. The bifurcation into the neck and no-neck curves occurs as soon as the trajectory for the system reaches the critical distance ($s=1.73$ fm). Clearly, the inclusion of the neck has a dramatic influence on the lifetime distribution for both systems by displacing the critical l wave for trapping of the ion-ion complex to higher incident angular momenta. This increases the complete-fusion cross section substantially. It is interesting that for the ^{20}Ne + ^{197}Au reactions no complete fusion is predicted in the absence of a neck, whereas substantial complete fusion is predicted when a neck is allowed to form. Since the data seem to display a substantial fusion-fission component, this is perhaps an indication of the importance of neck formation. The complete fusion events are treated here according to the method outlined in Ref. 35.

B. Potential energies and N/Z equilibrium

The dynamically averaged effective potential energies along the line of N/Z equilibrium for the ^{20}Ne + ^{nat}Cu and ^{20}Ne + ^{197}Au systems as a function of asymmetry are shown in Figs. 12 and 13. These figures illustrate an important difference between the ^{20}Ne + ^{nat}Cu and ^{20}Ne + ^{197}Au systems,

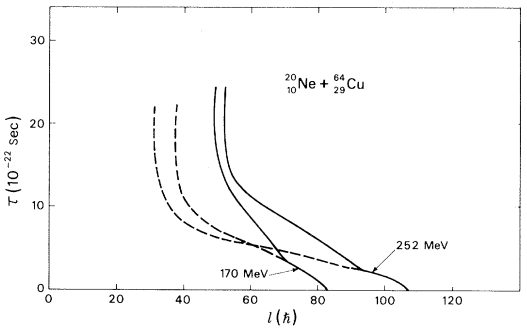

FIG. 10. Calculated average lifetimes for diffusion as a function of incident l wave for the ^{20}Ne + ^{64}Cu reactions. The solid and dashed lines are, respectively, for calculations with and without neck formation.

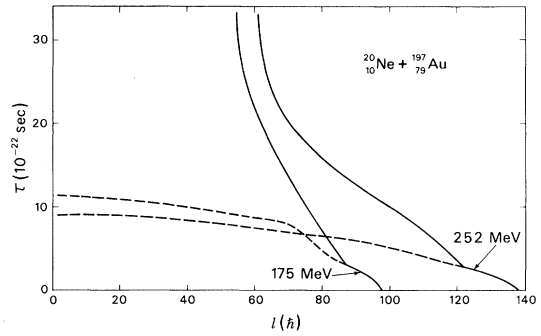

FIG. 11. Calculated average diffusion lifetimes as a function of incident l wave for the ^{20}Ne + ^{197}Au reactions. See Fig. 10.

which can explain the dramatic differences observed in their charge distributions near symmetry. For low l waves the driving force for diffusion in the ^{20}Ne + ^{nat}Cu reaction is toward the compound nucleus (greater asymmetry). This effect is diminished and is eventually reversed for higher l waves where the rotational energy produces a minimum at symmetry. On the other hand, for the Ne + Au reaction, the potential always exhibits a minimum at symmetry. However, this latter system may be first driven towards asymmetries greater than that of the entrance channel because of the rapid N/Z equilibration process. Typical N/Z equilibration times τ_{NZ} from Eq. (4), are about 10^{-22} sec, usually much shorter than the interaction times shown on Fig. 11. The equilibrium Z value due to N/Z equilibration for the ^{20}Ne + ^{197}Au reactions is 8. This increase of the initial asymmetry may push the ^{20}Ne + ^{197}Au system over the Businaro-Gallone mountain (see Fig. 13). Thus the driving force for diffusion would then be towards compound nucleus formation rather than towards symmetry.

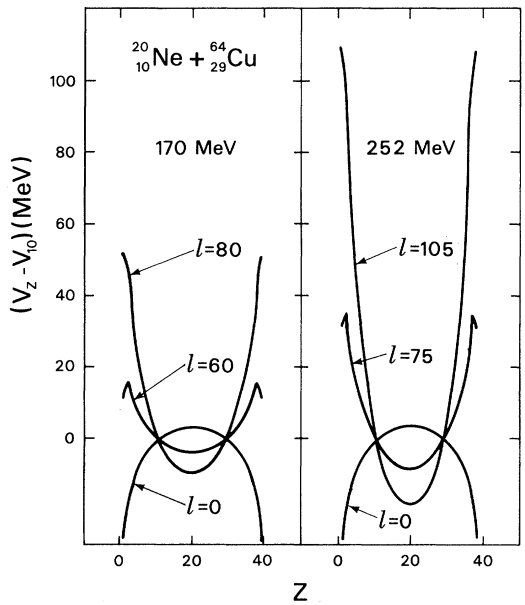

FIG. 12. Calculated total effective potential energies as a function of asymmetry for the ^{20}Ne + ^{64}Cu reactions.

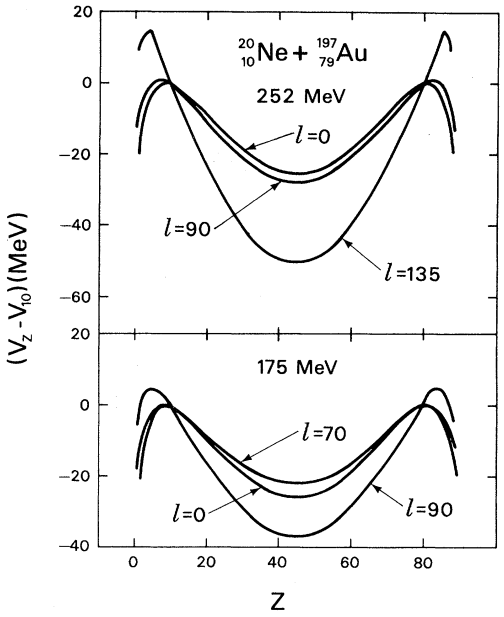

FIG. 13. Calculated total effective potential energies as a function of asymmtery for the ^{20}Ne + ^{197}Au reactions.

The driving force toward symmetry increases for both systems with increasing bombarding energy so that the effect of the N/Z equilibration should be compensated to some effect. For the ^{20}Ne + ^{nat}Cu systems, the effect of N/Z equilibration and of the potential energies shown here is such that the trapped l waves will mostly populate the compound nucleus asymmetry, and therefore contribute to the evaporation residue cross section. On the other hand, Ne + Au collisions will also populate a symmetric fusion-fission-like component to an extent similar to that observed experimentally. Of course, compound nucleus formation followed by fission will also contribute to the symmetric component. From Figs. 10 and 11 a critical angular momentum for complete fusion can be estimated from the angular momentum at which the lifetime becomes infinite. These angular momenta are: $l_{cr} \simeq 49\hbar$ for 170-MeV ^{20}Ne + ^{nat}Cu, $l_{cr} \simeq 53\hbar$ for

252-MeV ^{20}Ne + ^{nat}Cu, $l_{cr} \simeq 55\hbar$ for 175-MeV ^{20}Ne + ^{197}Au, and $l_{cr} \simeq 60\hbar$ for 252-MeV ^{20}Ne + ^{197}Au. The evaporation residue cross section has been measured[2] for 166-MeV ^{20}Ne + ^{63}Cu to be (1276±80) mb implying $l_{cr} = (60 \pm 1)\hbar$. This is somewhat higher than the estimate from the dynamical calculation suggesting that neck formation or energy dissipation may be more efficient than that given by this schematic model. On the other hand, this discrepancy could also arise if diffusion toward greater asymmetries by higher l waves substantially contributes to the apparent evaporation residue yield (essentially incomplete fusion reactions).

C. Angular distributions

In Figs. 14 and 15 experimental and calculated angular distributions are shown for representative fragment Z values both above and below the projectile. It should be noted that these calculated angular distributions have not been normalized. In fact there is only one free parameter in these calculations which is the ratio of the variance of the reaction lifetime to its mean value, σ^2/τ. Changing this variable adjusts the slope of the angular distributions for atomic numbers near the projectile. A value of $\sigma^2/\tau = 0.10$ yielded the best fits for the ^{20}Ne + ^{nat}Cu reactions, while $\sigma^2/\tau = 0.20$ appeared more appropriate for the ^{20}Ne + ^{197}Au reaction. These values correspond to fairly narrow lifetime distributions. The model calculations have not been corrected for charged-particle evaporation which may have shifted these data by as much as one to three charge units.[6,7,20] Probably, the most meaningful comparison with experiment is then at the lower bombarding energy and for products

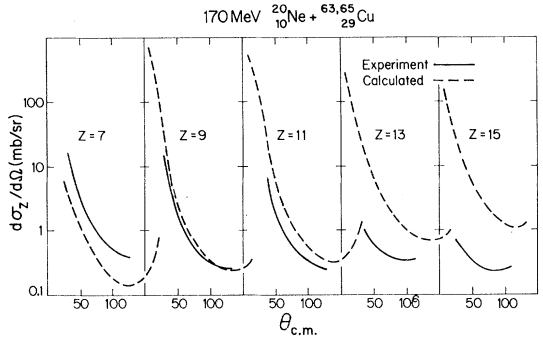

FIG. 14. Calculated and experimental angular distributions for representative products for the ^{20}Ne + ^{nat}Cu reactions.

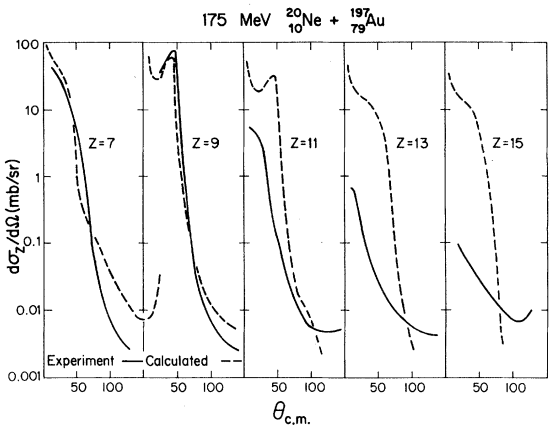

FIG. 15. Calculated and experimental angular distributions for representative products for the ^{20}Ne + ^{197}Au reactions.

close to the projectile Z value where the average energy loss (and hence, charged-particle evaporation) is least.

The trends observed in the data (side or forward peaking near the projectile Z value followed by a transition to $1/\sin\theta$ behavior above the projectile) are present in the calculations (see Figs. 14 and 15). The addition of neck formation was necessary in the ^{20}Ne + ^{nat}Cu systems to reproduce the observed flattening of the distribution at backward angles (see Fig. 14). Although some flattening in the ^{20}Ne + ^{nat}Cu distribution could be achieved by selecting a rather broad lifetime distribution (instead of a long-lived component), such a distribution does not produce the correct slope of the angular distribution in the forward hemisphere. It is particularly satisfying that the side peak in the 175-MeV ^{20}Ne + ^{197}Au data emerges from the model calculations (see Fig. 15). It is also interesting that the flattening of the distribution at backward angles is less pronounced in the ^{20}Ne + ^{197}Au data. This is predicted by the model simply because for higher l waves the fragments do not penetrate deeply enough to form a neck, which would increase the collision lifetime. Nevertheless, for a large range of l waves a neck eventually does form (see Fig. 11) leading to a symmetric compound-nucleus fission component in the charge distribution similar to that observed in the data.

The deviations of the calculation from the data for atomic numbers removed from the projectile has been a consistently puzzling feature of these data. The tendency is to overproduce nuclei heavier than the projectile and underproduce nuclei lighter than the projectile. This effect is perhaps most dramatically represented in the angle-

integrated charge distributions. Figure 16 shows the calculated and experimental charge distribution for the 170-MeV ^{20}Ne + ^{nat}Cu reaction. The fact that this discrepancy does not appear reconcilable by any reasonable variation of the dynamical variables in the model and that it appears so dramatically in the charge distributions (for which many of the details of the dynamics have been integrated out) suggests that it may relate to more fundamental considerations. It is possible that this effect may be due to changes in the potential energy surface when more realistic configurations are involved, or that it may require a more detailed understanding of the microscopic transition probabilities.

To some extent these deviations can be attributed to charged particle evaporation. In the ^{20}Ne + ^{nat}Cu reaction, particle emission would cause a reduction in the backward angle yield for products heavier than the projectile and a corresponding increase of lighter products, an effect which is observed in the data. Because of the different shape of the potential energy versus asymmetry (and hence, the different preevaporation yields) the opposite effect should occur at backward angles for the ^{20}Ne + ^{197}Au reaction products. For this system, charged particle evaporation should cause an increase in the calculated backward angle yield of lighter fragments as yields from the symmetric fission components are mixed in. This also is consistent with the data.

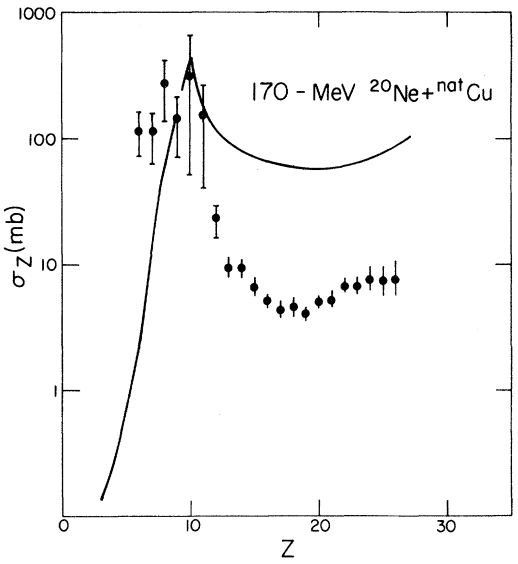

FIG. 16. Calculated and experimental angle-integrated charge distributions for the 170-MeV ^{20}Ne + ^{nat}Cu reaction.

VIII. CONCLUSION

In summary, we have presented data for ^{20}Ne-induced reactions with a light target (^{nat}Cu) and a heavy target (^{197}Au) at two bombarding energies. These data have been interpreted in the framework of a diffusion model in which nearly all of the free parameters have been eliminated by treating the dynamics explicitly. Two important additions to the model have been introduced to achieve a reasonable reproduction of the data. First of all, the influence of shape evolution has been included to increase the collision lifetimes and produce more complete fusion events. Secondly, the evolution of the Z distribution towards (N/Z) equilibrium has also been included to enhance the drift toward greater asymmetries. In this way, we believe that we have achieved at least a qualitative understanding of most of the features of these data. To quantitatively reproduce the data, more detailed calculations are needed which include more realistic nuclear shapes, particle evaporation, and such effects as the coupling of fluctuations in the mass transport to the evolution of the system. Some efforts along these lines are currently underway.[36]

ACKNOWLEDGMENTS

The authors extend their thanks to R. Babinet, J. Galin, R. Jared, and P. Russo for their contributions to various aspects of this work. This work was supported by the U. S. Department of Energy under Contract No. W-7405-ENG-48.

*Present address: Department of Nuclear Engineering, Technion-Israel Institute of Technology, Haifa, Israel.
†Present address: D.PH-N/MF-CEN, Saclay, France.
‡Present address: Department of Chemistry and Cyclotron Institute, Texas A&M Universtiy, College Station, Texas 77843.
§Present address: Math and Computing Division, Lawrence Berkeley Laboratory, Berkeley, California

94720.
[1]F. E. Obenshain, R. L. Ferguson, M. L. Halbert, D. C. Hensley, H. Nakahara, F. Plasil, F. Pleasonton, A. H. Snell, and R. G. Stokstad, Phys. Rev. C 18, 764 (1978).
[2]R. A. Dayras, R. G. Stokstad, D. C. Hensley, and M. L. Halbert, Phys. Rev. C 22, 1485 (1980).
[3]R. Babinet, L. G. Moretto, J. Galin, R. Jared, J. Moulton, and S. G. Thompson, Nucl. Phys. A258, 172 (1976).
[4]P. Glässel, R. S. Simon, R. M. Diamond, R. C. Jared, I. Y. Lee, L. G. Moretto, J. O. Newton, R. Schmitt, and F. S. Stephens, Phys. Rev. Lett. 38, 331 (1977).
[5]R. A. Dayras, R. G. Stokstad, C. B. Fulmer, D. C. Hensley, M. L. Halbert, R. L. Robinson, A. H. Shell, D. G. Sarantites, L. Westerberg, and J. H. Barker, Phys. Rev. Lett. 42, 697 (1979).
[6]R. P. Schmitt, G. Bizard, G. J. Wozniak, and L. G. Moretto, Phys. Rev. Lett. 41, 1152 (1978).
[7]R. P. Schmitt, G. J. Wozniak, G. U. Rattazzi, G. J. Mathews, R. Regimbart, and L. G. Moretto, Phys. Rev. Lett. 46, 522 (1981).
[8]M. L. Halbert, R. A. Dayras, R. L. Ferguson, F. Plasil, and D. G. Sarantites, Phys. Rev. C 17, 155 (1978).
[9]V. E. Viola, Jr., R. G. Clark, and W. G. Meyer, Nucl. Phys. A261, 174 (1976).
[10]G. J. Mathews, G. J. Wozniak, R. P. Schmitt, and L. G. Moretto, Z. Phys. A 283, 247 (1977).
[11]L. G. Moretto, and R. P. Schmitt, J. Phys. Suppl. C 5, 109 (1976).
[12]J. S. Sventek, Ph. D. thesis, University of California, Lawrence Berkeley Laboratory Report No. LBL-8407, 1978.
[13]L. G. Moretto, and J. S. Sventek, Phys. Lett. 58B, 26 (1975).
[14]L. G. Moretto, J. Phys. Soc. Jpn. Suppl. 44, 361 (1978).
[15]M. M. Fowler, and R. C. Jared, Nucl. Instrum. Methods 124, 341 (1975).
[16]L. C. Northcliffe, and R. F. Schilling, Nucl. Data Tables A7, 1 (1970).
[17]P. Glässel, R. C. Jared, and L. G. Moretto, Nucl. Instrum. Methods 142, 569 (1977).
[18]J. B. Moulton, Ph.D. thesis, University of California, Lawrence Berkeley Laboratory Report No. LBL-7717, 1978.
[19]D. J. Morrissey *et al.*, Lawrence Berkeley Laboratory Report No. LBL-13055, 1982.
[20]Jorge Gomez del Campo, in Proceedings of the Symposium on Heavy-Ion Physics from 10 to 200 MeV/*A*, Brookhaven National Laboratory, 1979, Brookhaven National Laboratory Report No. BNL-51115, 1979 (unpublished), Vol. 1, p. 83.
[21]C. K. Gelbke, C. Olmer, M. Buenerd, D. L. Hendrie, J. Mahoney, M. C. Mermaz, and D. K. Scott, Phys. Rep. 42, 311 (1978).
[22]M. Lefort and Ch. Ngo, Ann. Phys. (Paris) 3, 5 (1978).
[23]B. Gatty, D. Guerreau, M. Lefort, X. Tarrago, J. Galin, B. Cauvin, J. Girard, and H. Nifenecker, Nucl. Phys. A253, 511 (1975).
[24]L. G. Moretto, B. Cauvin, P. Glässel, R. Jared, P. Russo, J. Sventek, and G. Wozniak, Phys. Rev. Lett. 36, 1069 (1976).
[25]W. Norenberg, Phys. Lett. 52B, 289 (1974).
[26]J. Randrup, Nucl. Phys. A307, 319 (1978); A327, 490, (1979).
[27]J. Barrette and P. Braun-Munzinger, Nucl. Phys. A287, 195 (1977).
[28]L. G. Moretto, J. Sventek, and G. Mantzouranis, Phys. Rev. Lett. 42, 563 (1979).
[29]J. R. Birkelund, J. R. Huizenga, H. Freiesleben, K. L. Wolf, J. P. Unik, and V. E. Viola, Jr., Phys. Rev. C 13, 133 (1976).
[30]W. D. Myers, Nucl. Phys. A204, 465 (1973).
[31]W. J. Swiatecki, International School of Nuclear Physics, Erice-Trapani, Sicily, 1979, Lawrence Berkeley Laboratory Report No. LBL-8950.
[32]J. Randrup, Lawrence Berkeley Laboratory Report No. LBL-12676, Nucl. Phys. (to be published).
[33]J. P. Bløcki, Y. Boneh, J. R. Nix, J. Randrup, M. Robel, A. J. Sierk, and W. J. Swiatecki, Ann. Phys. (N.Y.) 113, 330 (1978).
[34]J. S. Sventek, and L. G. Moretto, Phys. Rev. Lett. 40, 697 (1978).
[35]G. J. Mathews and L. G. Moretto, Phys. Lett. 87B, 331 (1979).
[36]G. J. Mathews, J. Randrup, and L. G. Moretto, Lawrence Berkeley Laboratory Report No. LBL-10126 (unpublished).